Journal of Power Sources 275 (2015) 429–434

Contents lists available at ScienceDirect

Journal of Power Sources

journal homepage: www.elsevier.com/locate/jpowsour

Tracking inhomogeneity in high-capacity lithium iron phosphate batteries

William A. Paxton [a, *], Zhong Zhong [b], Thomas Tsakalakos [a]

[a] Materials Science and Engineering, Rutgers, The State University of New Jersey, Piscataway, NJ 08854, USA
[b] Photon Sciences, Brookhaven National Laboratory, Upton, NY 11973, USA

HIGHLIGHTS

- *In-situ* and *operando* profiling of a real-world 8 Ah lithium iron phosphate cell.
- Spatial tracking of inhomogeneity in three dimensions is achieved while discharging.
- Strong correlation between inhomogeneity evolution and cell overpotential is observed.
- Results suggests that particles contribute sequentially in order of connectivity.

GRAPHICAL ABSTRACT

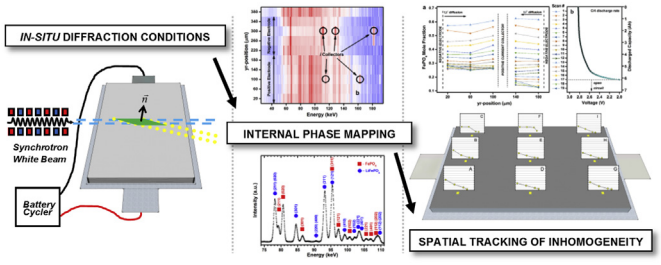

ARTICLE INFO

Article history:
Received 25 August 2014
Received in revised form
21 October 2014
Accepted 8 November 2014
Available online 11 November 2014

Keywords:
Inhomogeneity
X-ray diffraction
Lithium iron phosphate
Heterogeneous electrode
Characterization
In-situ

ABSTRACT

Energy-dispersive x-ray diffraction (EDXRD) is one of the few techniques that can internally probe a sealed battery under operating conditions. In this paper, we use EDXRD with ultrahigh energy synchrotron radiation to track inhomogeneity in a cycled high-capacity lithium iron phosphate cell under *in-situ* and operando conditions. A sequence of depth-profile x-ray diffraction spectra are collected with 40 μm resolution as the cell is discharged. Additionally, nine different locations of the cell are tracked independently throughout a second discharge process. In each case, a two-peak reference intensity ratio analysis (RIR) was used on the LiFePO4 311 and the FePO4 020 reflections to estimate the relative phase abundance of the lithiated and non-lithiated phases. The data provide a first-time look at the dynamics of electrochemical inhomogeneity in a real-world battery. We observe a strong correlation between inhomogeneity and overpotential in the galvanic response of the cell. Additionally, the data closely follow the behavior that is predicted by the resistive-reactant model originally proposed by Thomas-Alyea. Despite a non-linear response in the independently measured locations, the behavior of the ensemble is strikingly linear. This suggests that effects of inhomogeneity can be elusive and highlights the power of the EDXRD technique.

1. Introduction

The commercial introduction of lithium-ion batteries has enabled a worldwide portable-electronics revolution. More recently they are being used in much larger portable devices: hybrid gas/electric and electric vehicles. Lithium-ion batteries offer competitive properties (i.e. energy density, cycle life, and low self-discharge rates) which have proved advantageous for the

* Corresponding author. Department of Materials Science and Engineering, Rutgers, The State University of New Jersey, 607 Taylor Road, Piscataway, NJ 08854, USA.
E-mail address: will.paxton@rutgers.edu (W.A. Paxton).

http://dx.doi.org/10.1016/j.jpowsour.2014.11.035
0378-7753/

development of portable electronics [1]. However, for successful implementation in electric vehicle applications the current technological state of lithium-ion batteries needs improvement. Specifically, fire susceptibility and limited driving ranges of electric vehicles are pushing researchers and engineers to improve the durability, safety, and energy density of lithium-ion batteries [2].

Lithium iron phosphate ($LiFePO_4$) is an electrode material which offers a high cycle life, excellent thermal stability, and is composed of relatively earth abundant materials [3]. For these reasons, it is welcomed as the next-generation lithium-ion battery for electric vehicles. Structurally, $FePO_6$ octahedra combine with PO_4 tetrahedra to form a crystalline framework which can accommodate lithium intercalation. While the exact nature of lithium intercalation remains elusive, it is generally known lithium diffusion is one-dimensional and the transformation is biphasic, evident in its flat voltage profile [3].

Following its discovery by Padhi et al. 1997, lithium iron phosphate was regarded as a low-power material due to its poor intrinsic electronic and ionic conductivity [4]. Recently however, researchers have found that high-rate performance is possible with a reduction particle size and modification of surface chemistry [5,6]. Synthesizing nano-sized particles can reduce the bulk diffusion distances and adding a conductive surface coating improves intra-particle conductivity. With high-rate capability now achievable, lithium iron phosphate is a prime contender for use in electric vehicle batteries. However, with a theoretical energy density that is 30% less than well-established oxide electrodes (NCA) a formidable challenge for adoption remains.

For electric vehicles, theoretical energy density is still only one factor which influences driving range. A more applicable indicator of driving range would be the effective energy density of an entire battery pack. One strategy to improve effective energy density is to scale up the capacity of the electrochemical cell from which a battery is composed. By a simple calculation done in our lab, the energy density of an 8 Ah polymer pouch cell is 25% greater than that of an 18650 equivalent. Thus, cells produced with higher capacities (up to 100 Ah) could be advantageous to the electric vehicle industry allowing for simpler manufacturing, reduced battery-management overhead, and increased driving ranges.

Challenges still exist for high-capacity lithium ion cells, however. Specifically, the increase in size contributes to the complexity of their inner-working and behavior. Large cells are typically composed of multiple thin layers of current collectors, separators, electrodes, and electrolyte materials. When particulate electrodes exhibit large volume expansions from lithiation, electrochemical shock and fracture can occur [7]. Distributed across large areas and multiple layers, this can cause erratic and unpredictable current pathways which lead to cell inhomogeneity. Inhomogeneity is undesirable because it can cause under-utilization of electrode materials and create local areas of overcharge and overdischarge. This can ultimately reduce effective energy density and compromise cell safety and lifetime.

Past modeling efforts have predicted inhomogeneity in high capacity cells using multi-scale multi-dimensional modeling [8]. Additionally, numerous attempts have also been made to accurately model the phase transformation and voltage behavior for lithium iron phosphate batteries [9–16]. However, such modeling efforts should be met with experimental validation. Different attempts have been made to measure spatial variation and inhomogeneity in lithium ion batteries. Nanda et al. used Raman spectroscopy to map the state of charge of battery electrodes *ex situ* [17]. Liu et al. measured a large distribution of state of charge in a prismatic cell *ex situ* by synchrotron micro-diffraction [18]. Maire et al. provided state of charge mapping using an *in-situ* colorimetry method [19]. Zhang et al. developed a cell with multiple electrode tabs in an attempt to track *in-situ* current distribution in a lithium ion cell [20]. Within the last year, X-ray absorption spectroscopy measurements carried out by Ouvrard et al. and Katayama et al. have shown inhomogeneous reaction distributions [21,22]. Their results point towards variance in conductive networks as the origin of inhomogeneity observed. However, the measurements aren't made in real-world cells and don't provide resolution required for correlation to the voltage profile of the cell.

In this paper, we use a synchrotron white beam to conduct energy-dispersive x-ray diffraction (EDXRD) experiments in order to observe inhomogeneity in real-world high-capacity cells. EDXRD has proven to be a valuable tool for *in-situ* battery characterization [23–25]. Aided by ultrahigh photon energies, we are able to internally probe large lithium iron phosphate cells and collect diffraction spectra while discharging. By determining the relative amounts of non-lithiated and lithiated phases, we reveal the evolution of inhomogeneity with spatial and temporal resolution.

2. Experimental

2.1. Electrochemical cells

Two 8 Ah lithium iron phosphate polymer cells were chosen for this study. The cells were constructed in a prismatic layout consisting of multiple repeating units of electrodes, current collectors, and separator materials. The positive electrodes were comprised of nano-sized lithium iron phosphate and were treated with a carbonaceous coating. The negative electrodes were composed of graphitic carbon. Both cells were cycled approximately 1500 times with a 2C discharge rate and a 1C charge rate and were rested two days before the experiment.

2.2. Energy-dispersive x-ray diffraction

The energy-dispersive X-ray diffraction experiments were carried out at the superconducting wiggler beamline X17B1 of The National Synchrotron Light Source at Brookhaven National Laboratory in Upton, NY. The beamline provides a spectral flux with high brilliance across a range of energies up to 200 keV. The ultrahigh photon energies specifically allow for deep penetration in to the battery and minimal sample preparation; cells can be probed as-is. The cell was connected to a battery cycler (Arbin), and mounted to the sample stage. A germanium energy detector was fixed at 3° from the transmitted beam path. Bragg diffraction was measured in transmission (Laue) geometry, resulting in a fixed volume in space where diffraction occurs. A schematic is provided in Fig. 1 and the details of the beamline have been covered in this journal previously [24].

The incident and detector collimating slits were arranged such to form a gauge volume with dimensions of approximately 3 mm × 3 mm × 40 μm. The height of the gauge volume is commensurate with that of the individual layers in the cell and allows for a proper resolution across the electrochemical interface.

2.3. Stoichiometric determination

In order to determine the relative amounts of $FePO_4$ and $LiFePO_4$ present in the gauge volume, a semi-quantitative peak-fitting routine was employed. The $FePO_4$ (020) and the $LiFePO_4$ (311) reflections were chosen for their high intensities and minimal overlap with other reflections. For each diffraction spectra, the aforementioned peaks, and surrounding peaks, were fit with a Gaussian function and their integrated intensity was determined. The formula used to estimate the weight fraction for each phase is given below:

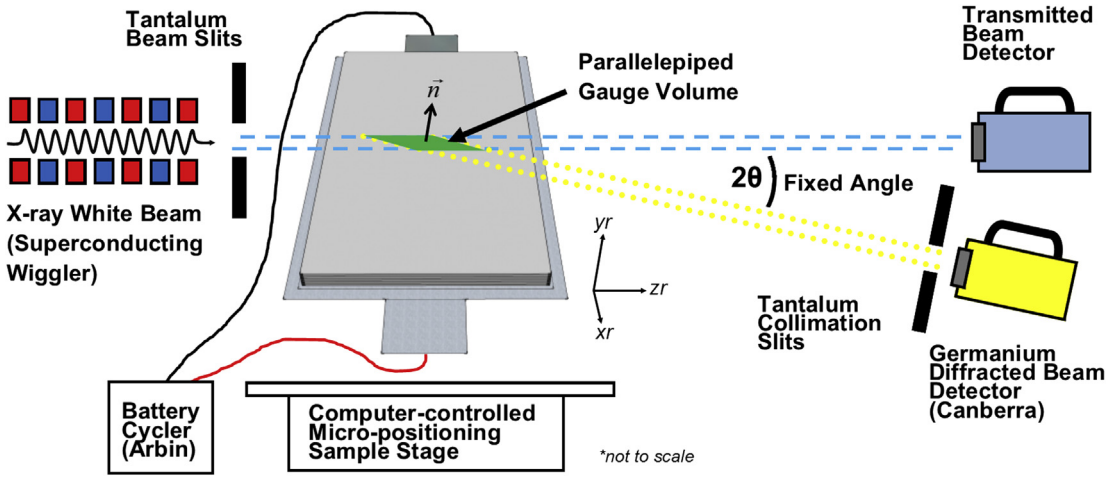

Fig. 1. Energy-dispersive synchrotron x-ray diffraction Schematic of the battery experiment at the X17B1 beamline at NSLS. Ultrahigh energy polychromatic x-rays are collimated through a series of slits and imposed on a battery which can move in all three dimensions. The transmission geometry gives way to a fixed volume in space where scattering is measured. The scattered x-rays are collected by a germanium energy detector after passing through collimating slits. The battery is connected to a cycler which is controlled by a computer.

$$\frac{W_\alpha}{W_\beta} = \frac{E_{\alpha,i}}{E_{\beta,j}} \frac{E^{rel}_{\beta,j}}{E^{rel}_{\alpha,i}} \frac{\mathrm{RIR}_{\beta,c}}{\mathrm{RIR}_{\alpha,c}}$$

where the W is the weight fraction, E is the measured intensity, E^{rel} is the relative intensity and RIR_c is reference intensity ratio to corundum [26]. For our analysis α is FePO4, β is LiFePO4, i is the 020 reflection and j is the 311 reflection. The reference intensity ratio (RIR_c and E^{rel}) values were provided by Jade and calculated from FIZ#99861 (09/11/09) for $FePO_4$ and calculated from FIZ#162282 (09/11/09) for $LiFePO_4$. Because we knew that the sum of the weight fractions is unity, we then solved for the W_α. Lastly, by diving by their molecular weights, we solved the mole fraction of each phase. The mole fraction of the $FePO_4$ phase serves as a useful as indicator for the local state of charge.

2.4. Measurement strategy

Entire mapping of a large cell would be time-prohibitive. So, in order to assess inhomogeneity, we devised two experimental conditions. First was to measure across the depth of an electrode interface located at the body-center of the cell. This was done in order to address variability in the yr-direction (See Fig. 1 for coordinate system). A series of diffraction spectra were collected across a pair of positive and negative electrodes in a cyclic fashion as the cell was discharged at a constant current. The resulting *operando* data provide space and time mapping of the electrode during discharge.

In a complimentary fashion, to address variability in the yr-plane, nine points were chosen to compare across the battery. With the second cell initially at 60% state of charge, the nine locations were probed at the positive electrode in the center of the prismatic stack. The cell was then discharged for 1 h at C/4 rate and the nine locations were probed again. This process was repeated two more times with the last discharge time being 25 min when the cell reached 2.0 V. Overall, the nine locations were measured four times throughout the discharge process and the discharge process was paused while the measurements were taken. Special care was taken to make sure that the same electrode plane was probed each time. This was accomplished by calibration procedure that involves scanning in the yr-direction each time the area was measured.

3. Results and discussion

In order to properly track inhomogeneity, a basic understanding of the internal structure of the battery is required. Starting at the body-center of the cell, one unit of the repeating layer structure was analyzed by taking 10 measurements across with 40 μm resolution. Shown in Fig. 2a, the data show both positive and negative electrode regions, divided by separators, with current collectors in the center of each electrode. The positive electrode is identified as lithium iron phosphate, the negative electrode as graphite, the positive collector foil as aluminum, and the negative foil as copper. A typical EDXRD spectra for the positive electrode is shown in Fig. 2b.

3.1. Depth profiling

Starting at approximately 75% of charge capacity, the cell was discharged at a C/4 rate while scanning across the 400 μm section shown in Fig. 2a. In total, 19 scans (where a scan is 10 spectra) were recorded operando as the cell was discharged. Focus was placed on the positive electrodes on either side of the current collector foil. Fig. 3a shows the mole fraction for the $FePO_4$ phase as a function of position and location on the discharge curve which is shown in Fig. 3b. The dashed lines represent the approximate locations of the negative electrodes and positive current collector. By tracking the local state of charge evolution on both sides of the current collector, Fig. 3a clearly shows the behavior on one side of the collector that is different from the opposite side. It is important to note that we recorded three data points on one side of the collector and two points on the other. We believe that this doesn't mean the electrode thicknesses are different but that the gauge volume was slightly off center with respect to the current collector.

We also notice that at any given location in Fig. 3a the response of the electrode is nonlinear. This is seen by the vertical spacing between each data point: as the cell is discharged, the spacing decreases, signifying that the local rate of reaction is slowing down. This asynchronous or delayed phenomenon has been observed before in numerous other $LiFePO_4$ studies [27–30]. One possible explanation for asynchronous behavior is a heterogeneous reaction and an x-ray probe volume which is not representative of the entire electrode. Our data supports this explanation showing that the

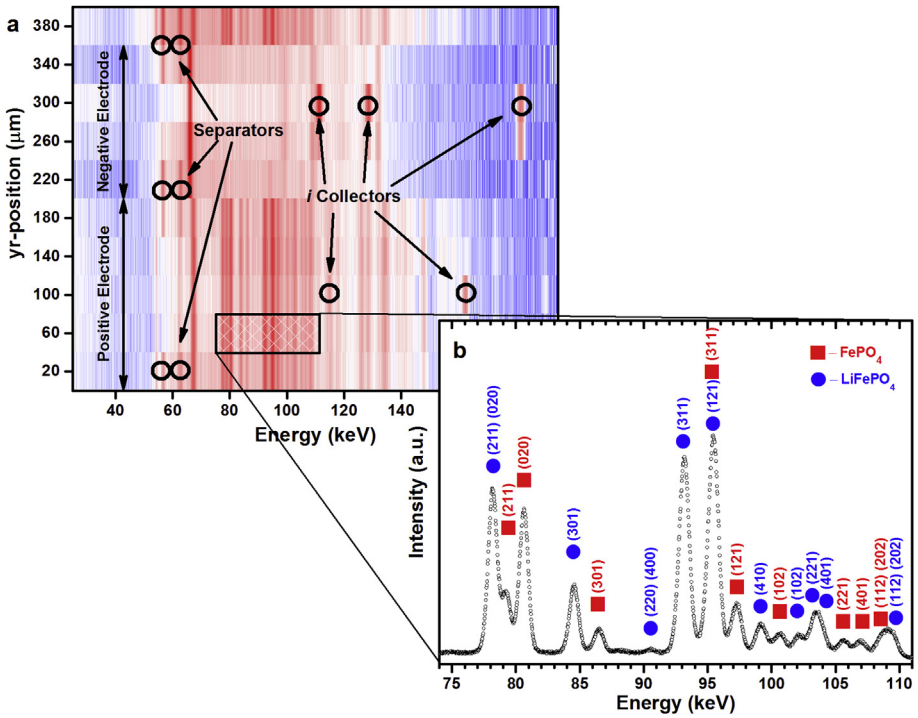

Fig. 2. Internal phase mapping and structural information a. Diffraction contour plot showing a one dimensional cross-section through an electrochemical cell. The region shown is one of approximately twenty repeating layers which comprise the cell. The contour plot is composed of ten diffraction spectra collected at 40 μm increments. Color represents the diffraction intensity with blue being the lowest and red being the highest. The current collectors are labeled and are coated on both sides with the respective electrode powders. b. Typical energy-dispersive diffraction spectrum of the lithium iron phosphate positive electrode. Upon lithiation, a new phase is created with a different crystal structure. This gives way to a juxtaposition of both diffraction patterns. The Bragg reflections of both phases are labeled by their *hkl* coordinates. (For interpretation of the references to color in this figure legend, the reader is referred to the web version of this article.)

asynchronous behavior is more pronounced on the side where the reaction range is more limited.

The last two scans were taken after the cell finished discharging and was at open circuit voltage. It is important to point out that in Fig. 3a at 20 μm and 140 μm, a phase relaxation is observed. That is that the local state of charge farthest from the current collector increases. This behavior has been observed before and suggests higher concentration of defects in those areas and/or non-equilibrium conditions [10,15,31].

Fig. 3b shows a voltage plateau around 2.8 V for the cell. We attribute the low voltage to a high internal resistance in the cell. Unfortunately, we did not collect voltage data after the discharge.

3.2. In-plane profiling

In order to characterize in-plane variability, nine points of interest were chosen and are shown in Fig. 4a. Starting at about 60% of charge capacity, the nine points were tracked throughout the discharge process. The results, shown in Fig. 4b, are very profound as the locally measured areas exhibit a high degree of

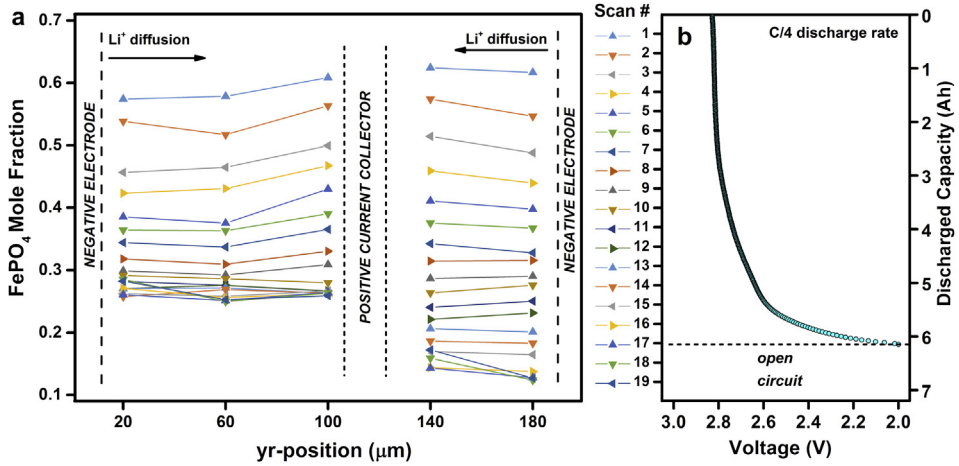

Fig. 3. *Operando* electrode mapping a. Time evolution of the iron phosphate mole fraction as a function of position (depth) in the electrode layer. As the cell is discharged, the iron phosphate phase is converted to lithium iron phosphate. The approximate locations for the positive current collector and negative electrodes are indicated. Lines are provided as a guide only. b. The cell potential as a function of capacity obtained while discharging the cell. The scan numbers on the left axis indicate the point at which each set of spectra were collected. Two scans were taken at open circuit after the discharge was halted.

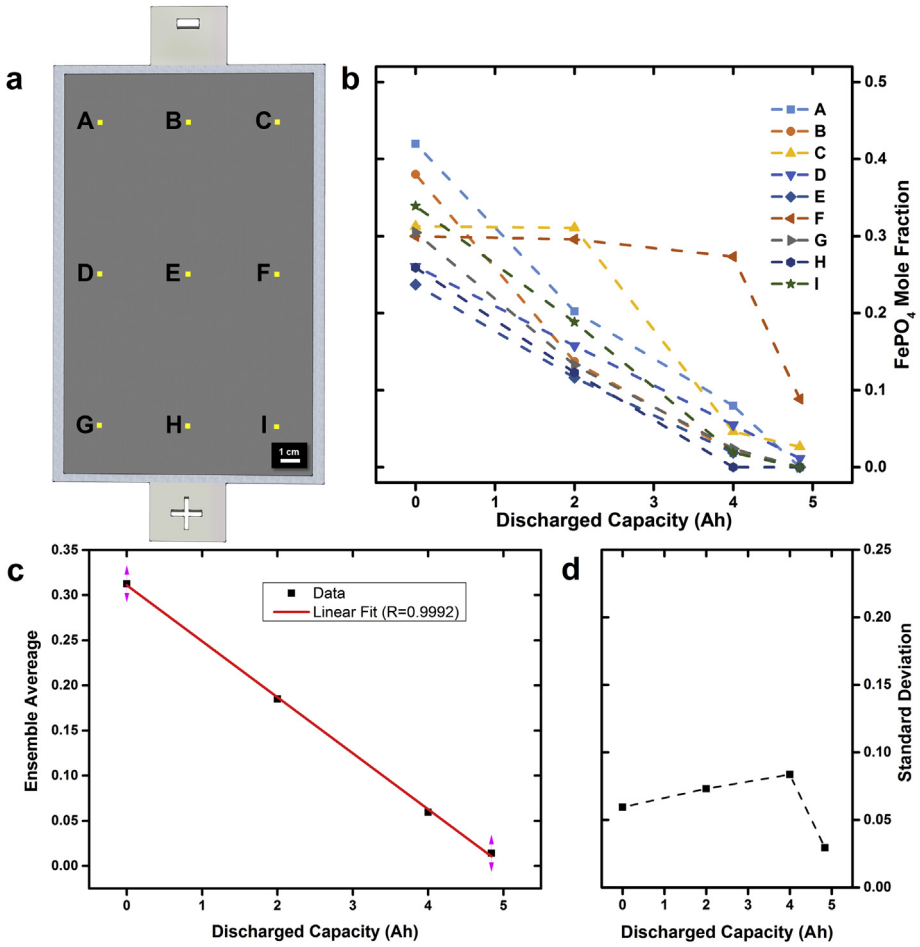

Fig. 4. Spatial inhomogeneity while discharging a. Schematic showing the locations of the battery that are probed. The yellow dots represent the area measured in the plane shown. b. Mole fraction of un-lithiated iron phosphate as a function of discharged capacity. As the cell is discharged the abundance of iron phosphate decreases. The mole fraction of iron phosphate can also be interpreted as the local state of charge in the cell. c. Evolution of the ensemble average as a function of discharged capacity. The data show extremely linear behavior with an R-value of 0.9992. d. Standard deviation of the ensemble versus discharged capacity.

inhomogeneity. Initially, all nine areas contain different local phase fractions. Once the discharge takes place, each location reacts at a different rate and the fastest are the locations (B, E, G) corresponding to the center of the cell, *e.g.* the space directly between the tabs.

Fig. 4c shows the average of the ensemble measured at each discharge state. The behavior is strikingly linear. While a sample size of nine may not be statistically significant, it still reveals an important characteristic of the $LiFePO_4$ system: a linear behavior of the ensemble juxtaposed with an inhomogeneous behavior of local regions. In light of this, care should be taken when comparing macroscopic and microscopic measurements *e.g.* studies of cells probed *in situ* by x-ray techniques where chemical composition data are then compared to the electrical response of the cell. In these cases, the total volume of the material probed by x-rays is most likely only a fraction of the volume of material contributing to the discharge curve. Therefore, extracting a $Li_{1-x}FePO_4$ line from the voltage curve and expecting a linear behavior in the chemical composition may result in asynchronous or delayed-discharge observation.

Most pronounced in the dataset is the delayed-discharge behavior of locations C and F. This behavior is characteristic lithium iron phosphate and is explained well by the resistive-reactant model originally proposed by Thomas-Alyea [12]. The model describes conductively coated LiFePO4 particles in terms of their inter- and intra-particle connectivity and proposes that they contribute in order of their conductivity. That is to say that the particles with the lowest electrical resistance react first and the ones with the highest resistance react last. Our observed behavior of locations C and F suggests that these areas have poorer electrical conductivity.

The standard deviation of the ensemble at different discharge states is shown in Fig. 4d. The deviation increases as the cell is discharged but when completely discharged the deviation is at a minimum. The resistive-reactant model has been further investigated by Safari et al. through modeling experiments. [13] In their paper, they model four particle groups with varying amounts of conductivity and follow them independently during a discharge. In our data, Fig. 4b and d follows almost exactly the work of Safari et al. in Fig. 11. They predict that the reaction networks formed through the heterogeneously connected particles is responsible for the path dependency of lithium iron phosphate batteries.

4. Conclusions

We have studied inhomogeneity in an 8 Ah high-capacity lithium iron phosphate cell using energy-dispersive x-ray diffraction with synchrotron radiation. Chemical composition was estimated through a reference intensity ratio method on the $LiFePO_4$ (311) and the $FePO_4$ (020) reflections. *Operando* electrode depth

profiling was achieved during discharge conditions and revealed asynchronous discharge behavior and incomplete electrode utilization. Additionally, in-plane electrode measurements were made *in-situ* while the cell was discharged. Inhomogeneous behavior was observed across nine in-plane regions and a severely delayed discharge occurred at two of the regions. Ensemble behavior is linear suggesting the importance of micro-versus macro-observations. Overall, we attribute the inhomogeneous behavior to heterogeneous conductive coating on the particles as the data follows the resistive-reactant model closely.

Acknowledgments

The authors gratefully acknowledge Ankur Choksi, and Bart Visser for their support in the laboratory. The authors also acknowledge General Electric for the use of use of their battery cycler and their efforts in improving the beamline. Use of the National Synchrotron Light Source, Brookhaven National Laboratory, was supported by the U.S. Department of Energy, Office of Science, Office of Basic Energy Sciences, under Contract No. DE-AC02-98CH10886.

References

[1] B. Scrosati, J. Garche, J. Power Sources 195 (2010) 2419–2430.
[2] Armand, Tarascon, Nature 451 (2008) 652–657.
[3] W. Zhang, J. Power Sources 196 (2011) 2962–2970.
[4] Padhi, J. Electrochem. Soc. 144 (1997) 1188.
[5] N. Ravet, Y. Chouinard, J.F. Magnan, S. Besner, M. Gauthier, M. Armand, J. Power Sources 97–98 (2001) 503–507.
[6] Yamada, Chung, Hinokuma, J. Electrochem. Soc. 148 (2001) A224–A229.
[7] Ebner, Marone, Stampanoni, Wood, Science 342 (2013) 716–720.
[8] Kim, Smith, Lee, Santhanagopalan, Pesaran, J. Electrochem. Soc. 158 (2011) A955–A969.
[9] Srinivasan, Newman, J. Electrochem. Soc. 151 (2004) A1517–A1529.
[10] Delmas, Maccario, Croguennec, Le Cras, Weill, Nat. Mater. 7 (2008) 665–671.
[11] G.K. Singh, G. Ceder, M.Z. Bazant, Electrochim. Acta 53 (2008) 7599–7613.
[12] K.E. Thomas-Alyea, ECS Trans. 16 (2008) 155–165.
[13] Safari, Delacourt, J. Electrochem. Soc. 158 (2011) A63–A73.
[14] Safari, Delacourt, J. Electrochem. Soc. 158 (2011) A562–A571.
[15] Malik, Zhou, Ceder, Nat. Mater. 10 (2011) 587–590.
[16] Farkhondeh, Safari, Pritzker, Fowler, Han, Wang, Delacourt, J. Electrochem. Soc. 161 (2013) A201–A212.
[17] J. Nanda, J. Remillard, A. O'Neill, D. Bernardi, T. Ro, K.E. Nietering, J. Go, T.J. Miller, Adv. Funct. Mater. 21 (2011) 3282–3290.
[18] Liu, Kunz, Chen, Tamura, Richardson, J. Phys. Chem. Lett. 1 (2010) 2120–2123.
[19] Maire, Evans, Kaiser, Scheifele, Novak, J. Electrochem. Soc. 155 (2008) A862.
[20] Zhang, Shaffer, Wang, Rahn, J. Electrochem. Soc. 160 (2013) A610–A615.
[21] G. Ouvrard, M. Zerrouki, P. Soudan, B. Lestriez, C. Masquelier, M. Morcrette, S. Hamelet, S. Belin, A.M. Flank, F. Baudelet, J. Power Sources 229 (2013) 21.
[22] M. Katayama, K. Sumiwaka, R. Miyahara, H. Yamashige, H. Arai, Y. Uchimoto, T. Ohta, Y. Inada, Z. Ogumi, J. Power Sources 269 (2014) 999.
[23] Scarlett, Madsen, Evans, Coelho, McGregor, Rowles, Lanyon, Urban, J. Appl. Crystallogr. 42 (2009) 502–512.
[24] J. Rijssenbeek, Y. Gao, Z. Zhong, M. Croft, N. Jisrawi, A. Ignatov, T. Tsakalakos, J. Power Sources 196 (2011) 2332–2339.
[25] Takeuchi, Marschilok, Takeuchi, Ignatov, Zhong, Croft, Energy & Environ. Sci. 6 (2013) 1465.
[26] R.L. Snyder, Powder Diffr. 7 (1992) 186–193.
[27] H. Chang, C. Chang, H. Wu, M. Yang, H. Sheu, N. Wu, Electrochem. Commun. 10 (2008) 335–339.
[28] Leriche, Hamelet, Shu, Morcrette, Masquelier, Ouvrard, Zerrouki, Soudan, Belin, Elkaïm, Baudelet, J. Electrochem. Soc. 157 (2010) A606–A610.
[29] Wang, Jaye, Nam, Zhang, Chen, Bai, Li, Huang, Fischer, Yang, J. Mater. Chem. 21 (2011) 11406.
[30] H.C. Shin, K.W. Nam, W.Y. Chang, B.W. Cho, W. Yoon, X. Yang, K.Y. Chung, Electrochim. Acta 56 (2011) 1182–1189.
[31] Park, Kameyama, Yao, Electrochem. Solid State Lett. 15 (2012) A49–A52.